Journal of Organometallic Chemistry 694 (2009) 3902–3911

Contents lists available at ScienceDirect

Journal of Organometallic Chemistry

journal homepage: www.elsevier.com/locate/jorganchem

Synthesis, structure, properties, volatility, and thermal stability of molybdenum(II) and tungsten(II) complexes containing allyl, carbonyl, and pyrazolate or amidinate ligands

Oussama M. El-Kadri [1], Mary Jane Heeg, Charles H. Winter *

Department of Chemistry, Wayne State University, 5101 Cass Avenue, Detroit, MI 48202, USA

ARTICLE INFO

Article history:
Received 24 June 2009
Received in revised form 3 August 2009
Accepted 4 August 2009
Available online 8 August 2009

Keywords:
Molybdenum
Tungsten
Amidinate ligand
Pyrazolate ligand
Atomic layer deposition

ABSTRACT

Treatment of M(allyl)(Cl)$(CO)_2(py)_2$ (M = Mo, W) with 1 equiv. of potassium pyrazolates in tetrahydrofuran at −78 °C afforded M(allyl)$(R_2pz)(CO)_2(py)_n$ (R_2pz = 3,5-disubstituted pyrazolate; n = 1, 2) in 68–81% yields. X-ray crystal structure analyses of Mo(allyl)$((CF_3)_2pz)(CO)_2(py)_2$ and W(allyl)$(tBu_2pz)(CO)_2(py)$ revealed η^1- and η^2-coordination of the $(CF_3)_2pz$ and tBu_2pz ligands, respectively. Analogous treatment of Mo(allyl)(Cl)$(CO)_2(NCCH_3)_2$ with 1 equiv. of tBu_2pzK in tetrahydrofuran at −78 °C afforded [Mo(allyl)$(tBu_2pz)(CO)_2]_2$ in 79% yield. An X-ray crystal structure analysis of [Mo(allyl)$(tBu_2pz)(CO)_2]_2$ showed a dimeric structure bridged by two μ-η^2:η^1-tBu_2pz ligands. Treatment of M(allyl)(Cl)$(CO)_2(py)_2$ with 1 equiv. of lithium 1,3-diisopropylacetamidinate or lithium 1,3-di-*tert*-butylacetamidinate in diethyl ether at −78 °C afforded M(allyl)(iPrNC(Me)NiPr)$(CO)_2(py)$ and M(allyl)(tBuNC(Me)NtBu)$(CO)_2(py)$, respectively, in 68–78% yields. The new complexes were characterized by spectral and analytical methods and by X-ray crystal structure determinations. M(allyl)(iPrNC(Me)NiPr)$(CO)_2(py)$ adopt pseudo-octahedral geometry about the metal centers, with the 1,3-diisopropylacetamidate ligand nitrogen atoms spanning one axial site and one equatorial site of the octahedron. By contrast, M(allyl)(tBuNC(Me)NtBu)$(CO)_2(py)$ adopt pseudo-octahedral structures in which the two 1,3-di-*tert*-butylacetamidinate ligand nitrogen atoms span two equatorial coordination sites. Sublimation of M(allyl)(tBuNC(Me)NtBu)$(CO)_2(py)$ at 105 °C/0.03 Torr afforded ⩽7% yields of M(allyl)(tBuNC(Me)NtBu)$(CO)_2$, along with sublimed M(allyl)(tBuNC(Me)NtBu)$(CO)_2(py)$. W(allyl)(tBuNC(Me)NtBu)$(CO)_2$ exists in the solid state as a 16-electron complex with distorted square pyramidal geometry. Many of the new complexes undergo dynamic ligand site exchange in solution, and these processes were probed by variable temperature ^{1}H NMR spectroscopy. The volatilities and thermal stabilities were evaluated to determine the potential of the new complexes for use as precursors in thin film growth experiments.

1. Introduction

Molybdenum(II) and tungsten(II) complexes containing the *fac*-M(allyl)$(CO)_2$ fragment have been widely investigated to establish their chemical properties [1–4]. Additionally, they have been explored as catalysts in organic synthesis [5]. A particularly useful aspect of these complexes is that the *fac*-M(allyl)$(CO)_2$ fragment is relatively stable, and is maintained through many reactions that occur within the coordination sphere. We have recently reported the atomic layer deposition (ALD) growth of W_2O_3 films using the tungsten(III) precursor $(Me_2N)_3WW(NMe_2)_3$ and water as precursors [6]. This work demonstrated that the metal precursor oxidation state may determine the metal oxidation state in the thin film material in ALD growth. Retention of the precursor oxidation state in the thin film material is very rare in film growth by ALD and chemical vapor deposition (CVD) [7]. To extend this concept, we sought to develop new ALD precursors that might be employed for the growth of low valent molybdenum and tungsten oxide phases. In ALD, two or more precursors are introduced sequentially into the deposition chamber, and are separated by an inert gas purge that removes excess precursor as well as reaction byproducts [8]. This pulse sequence results in film growth by self-limiting surface reactions, and allows the film thickness to be precisely controlled by adjusting the number of deposition cycles. ALD requires precursors that are thermally stable at the substrate temperature to avoid loss of the self-limited growth mechanism [8]. Recent reports have demonstrated that pyrazolate [9] or amidinate [10] ligands increase the thermal stability of metal complexes, and that the enhanced thermal stability of these complexes makes them

* Corresponding author. Tel.: +1 (313) 577 5224; fax: +1 (313) 577 8289.
E-mail address: chw@chem.wayne.edu (C.H. Winter).
[1] Present address: Department of Biology and Chemistry, American University of Sharjah, P.O. Box 26666, Sharjah, United Arab Emirates.

0022-328X/$ - see front matter © 2009 Elsevier B.V. All rights reserved.
doi:10.1016/j.jorganchem.2009.08.001

very useful precursors for ALD film growth. Yamaguchi has described the synthesis and properties of molybdenum and tungsten complexes of the formula M(allyl)(X)$(CO)_2$(py), where X is an N-aryl-substituted formamidinate or acetamidinate ligand [2]. These complexes are conveniently available through salt metathesis reactions from the easily prepared starting materials M(allyl)(Cl)$(CO)_2(py)_2$ [2]. Since the M(allyl)$(CO)_2$ fragment may have high thermodynamic stability [1–5], we sought to prepare complexes containing M(allyl)$(CO)_2$ moieties and pyrazolate or amidinate ligands. Such complexes might lead to new classes of ALD precursors. Herein, we describe the synthesis, structure, dynamic NMR spectra, volatility, and thermal stability of molybdenum(II) and tungsten(II) complexes of the formula M(allyl)(X)$(CO)_2(py)_n$ and $[M(allyl)(X)(CO)_2]_2$, where X is an amidinate or pyrazolate ligand and $n = 0$, 1, or 2.

2. Results and discussion

Treatment of M(allyl)(Cl)$(CO)_2(py)_2$ [2a,11] with 1 equiv. of potassium 3,5-bis(trifluoromethyl)pyrazolate ($(CF_3)_2$pzK) or potassium 3,5-di-*tert*-butylpyrazolate (tBu_2pzK) in tetrahydrofuran at −78 °C afforded **1a**, **1b**, **2a**, and **2b** as yellow crystalline solids in 68–81% yields (Eq. (1)). The formulations of these complexes were based upon spectroscopic and analytical techniques, and by X-ray crystal structure determinations. The solid state structure of **1a** contains a monomeric metal center attached to one η^3-allyl, one η^1-pyrazolate, two pyridine, and two carbonyl ligands. The geometry about the molybdenum center is pseudo-octahedral, if the η^3-allyl ligand is considered to occupy one coordination site. Two carbonyl ligands, one pyridine ligand nitrogen atom, and one pyrazolate ligand nitrogen atom form the equatorial plane of the octahedron, while one pyridine ligand and the η^3-allyl ligand comprise the axial sites. The carbonyl stretches in the infrared spectrum of **1a** appeared at 1944 and 1847 cm^{-1}, while those of **1b** were observed at 1937 and 1852 cm^{-1}. Complexes **2a** and **2b** also adopt monomeric, pseudo-octahedral structures, in which each metal ion is bonded to one η^3-allyl, one η^2-pyrazolate, one pyridine, and two carbonyl ligands. The two carbonyl ligands, one pyridine ligand, and one nitrogen atom from the η^2-pyrazolate ligand define the equatorial plane of the octahedron. Carbonyl stretching frequencies were observed in the infrared spectra at 1941 and 1842 cm^{-1} for **2a** and 1931 and 1828 cm^{-1} for **2b**. Detailed variable temperature ^{1}H NMR studies were carried out for **1a**, **1b**, **2a**, and **2b** and are discussed below.

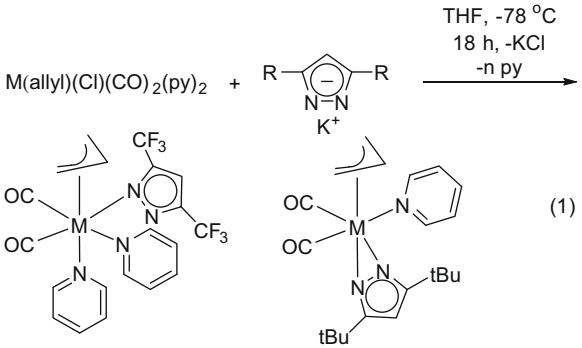

The dimeric complex **3a** was obtained as red crystals by treatment of Mo(allyl)(Cl)$(CO)_2(NCCH_3)_2$ [12] with 1 equiv. of tBu_2pzK in tetrahydrofuran at −78 °C (Eq. (2)). The composition and structure of **3a** were established by a combination of spectroscopic and analytical techniques, and by an X-ray crystal structure determination. The tungsten analog **3b** was prepared, but it was obtained in low yields and impure form despite many attempts to optimize its synthesis. As such, **3b** was not pursued further. Each molybdenum atom in the dimer of **3a** is bonded to one η^3-allyl and two carbonyl ligands. The dimer is bridged by two μ-η^2:η^1-pyrazolate ligands. The infrared spectrum of **3a** showed two absorptions for the carbonyl ligands at 1935 and 1845 cm^{-1}. The variable temperature ^{1}H NMR spectra of **3a** are complex, and are discussed below.

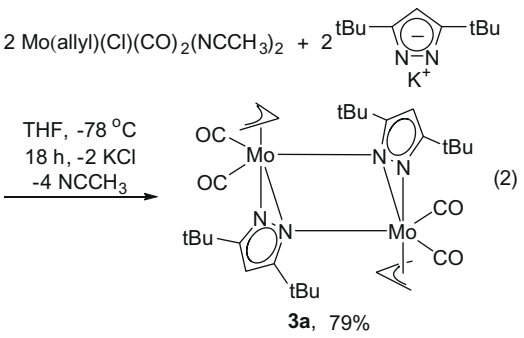

Similar synthetic approaches were used to prepare molybdenum and tungsten complexes containing amidinate ligands. Treatment of M(allyl)(Cl)$(CO)_2(py)_2$ (M = Mo, W) with 1 equiv. of a lithium amidinate salt (prepared in situ from the corresponding carbodiimide and methyllithium) in diethyl ether at −78 °C afforded **4a**, **4b**, **5a**, and **5b** as yellow crystalline solids in 68–87% yields (Eq. (3)). The formulations of these complexes were based upon spectroscopic and analytical techniques. In addition, an X-ray crystal structure determination was carried out for **4b**. Like **1a**, **2a**, and **2b**, the solid state structure of **4b** revealed a monomeric, pseudo-octahedral tungsten center coordinated to one η^3-allyl, one η^2-amidinate, one pyridine, and two carbonyl ligands. In **4b**, the equatorial plane of the octahedron is defined by two carbonyl ligands, one pyridine ligand, and one nitrogen atom from the amidinate ligand. As detailed below, the solution structures of **5a** and **5b** are ones in which the equatorial plane of the octahedron is defined by two carbonyl ligands and the two nitrogen atoms from the amidinate ligand. Complexes **4a**, **4b**, **5a**, and **5b** each showed two strong carbonyl absorptions in the infrared spectra, with one between 1905 and 1917 cm^{-1} and the other between 1803 and 1818 cm^{-1}. Variable temperature ^{1}H NMR spectra for **4a**, **4b**, **5a**, and **5b** are described below.

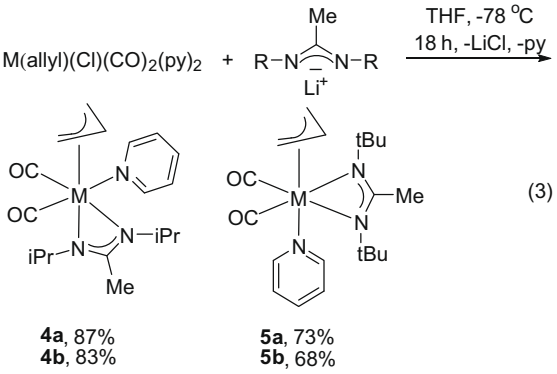

Sublimation of **5a** and **5b** afforded unchanged **5a** and **5b** in addition to trace amounts (⩽7%) of Mo(allyl)(tBuNC(Me)NtBu)$(CO)_2$ (**6a**) and W(allyl)(tBuNC(Me)NtBu)$(CO)_2$ (**6b**) as dark orange crystals. Subli-

mation of **5a** at 105 °C/0.03 Torr afforded only a few crystals of dark orange **6a**, mixed in with yellow crystals of **5a**. The solid state structure of **6a** was determined by X-ray crystallography, but it was not possible to characterize it further due to the very small amounts that were obtained. As outlined in equation 4, sublimation of **5b** at 105 °C/0.03 Torr afforded yellow crystals of **5b** (20% yield) and dark orange crystals of **6b** (7% yield). There was a 50% non-volatile residue at the completion of the sublimation of **5b**, indicating that significant decomposition occurred. Manual separation of **5b** and **6b** under a microscope allowed isolation of about 100 mg of crystalline **6b**, mixed with 5–10% of **5b**. The 90–95% purity of **6b** allowed spectral characterization, but a satisfactory combustion analysis was not obtained. An X-ray crystal structure confirmed the formulation of **6b** as a 16-electron complex containing an η^3-allyl ligand, two carbonyl ligands, and an η^2-amidinate ligand. Two carbonyl absorptions were observed in the infrared spectrum at 1922 and 1823 cm^{-1}. These values are similar to those observed for the 18-electron complexes **5a** and **5b**. The ^1H NMR spectra of **6b** are described below.

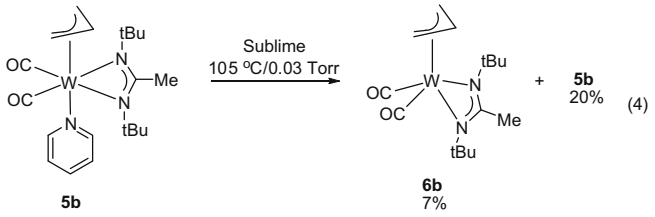

The crystal structures of **1a**, **2a**, **2b**, **3a**, **4b**, and **6b** were determined to establish the geometry about the metal centers and to assess the bonding modes of the various nitrogen donor ligands. Experimental crystallographic data are summarized in Table 1, selected bond lengths and angles are presented in Tables 2–6, and perspective views are given in Figs. 1–5. Since **2a** and **2b** are isostructural, only the data for **2b** are described herein. Also, the X-ray crystal structure of **6a** was determined. The structural data for **2a** and **6a** are contained in the Supplementary material.

Complexes **1a**, **2b**, **3a**, and **4b** possess pseudo-octahedral metal centers, with various combinations of carbon and nitrogen donor atoms. For simplicity, the η^3-allyl ligands are assumed to occupy one axial coordination site of the octahedra in **1a**, **2b**, **3a**, and **4b**. Since the ionic radii of molybdenum(II) and tungsten(II) are identical, bond lengths and angles can be compared directly. These complexes share common facially-arranged η^3-allyl and carbonyl ligands, with the open mouth of the allyl ligands pointed over the two carbonyl ligands. A similar arrangement of the η^3-allyl and two carbonyl ligands is observed in most structurally

Table 2
Selected bond lengths (Å) and angles (°) for **1a**.

Mo–N(1)	2.287(2)
Mo–N(3)	2.252(2)
Mo–N(4)	2.346(2)
Mo–C(6)	2.318(2)
Mo–C(7)	2.208(2)
Mo–C(8)	2.333(2)
Mo–C(9)	1.955(2)
Mo–C(10)	1.949(2)
N(1)–Mo–N(3)	83.79(5)
N(1)–Mo–N(4)	90.63(5)
N(1)–Mo–C(9)	97.95(7)
N(1)–Mo–C(10)	169.12(7)
N(3)–Mo–N(4)	80.21(6)
N(3)–Mo–C(9)	89.73(7)
N(3)–Mo–C(10)	86.10(7)
N(4)–Mo–C(9)	166.02(7)
N(4)–Mo–C(10)	91.61(7)
C(9)–Mo–C(10)	77.95(8)

Table 3
Selected bond lengths (Å) and angles (°) for **2b**.

W(1)–N(1)	2.224(2)
W(1)–N(2)	2.112(2)
W(1)–N(3)	2.286(2)
W(1)–C(12)	1.964(2)
W(1)–C(13)	1.940(2)
W(1)–C(14)	2.292(2)
W(1)–C(15)	2.202(3)
W(1)–C(16)	2.326(2)
N(1)–W(1)–N(2)	37.12(6)
N(1)–W(1)–N(3)	80.55(6)
N(1)–W(1)–C(12)	93.12(8)
N(1)–W(1)–C(13)	143.26(8)
N(2)–W(1)–N(3)	78.88(6)
N(2)–W(1)–C(12)	91.10(8)
N(2)–W(1)–C(13)	106.62(8)
N(3)–W(1)–C(12)	169.62(8)
N(3)–W(1)–C(13)	101.22(7)
C(12)–W(1)–C(13)	78.92(9)
W(1)–N(1)–C(1)	149.59(14)
W(1)–N(2)–C(3)	148.65(14)

Table 1
Crystal data and data collection parameters for **1a**, **2b**, **3a**, **4b**, and **6b**.

	1a	2b	3a	4b	6b
Empirical formula	$C_{20}H_{16}F_6MoN_4O_2$	$C_{21}H_{29}N_3O_2W$	$C_{32}H_{46}Mo_2N_4O_4$	$C_{18}H_{27}N_3O_2W$	$C_{15}H_{26}N_2O_2W$
Fw	554.31	539.32	742.61	501.28	450.23
Space group	*C2/c*	$P2_1/c$	$P2_1/c$	$P\bar{1}$	$P2_1/n$
a (Å)	18.5269(6)	17.9675(4)	10.5224(3)	8.2229(2)	9.8233(5)
b (Å)	15.6330(5)	14.7572(3)	10.5111(2)	10.5559(3)	11.6072(7)
c (Å)	15.0605(5)	18.4002(4)	15.6292(4)	12.0958(4)	14.8651(8)
α (°)				90.485(2)	
β (°)	92.4840(10)	115.3930(10)	105.5880(10)	102.4350(10)	99.759(2)
γ (°)				106.9150(10)	
V (Å^3)	4357.9(2)	4407.46(16)	1665.04(7)	978.08(5)	1670.41(16)
Z	8	8	2	2	4
T (K)	100(2)	100(2)	100(2)	100(2)	100(2)
λ (Å)	0.71073	0.71073	0.71073	0.71073	0.71073
ρ_{calc} (g cm^{-3})	1.690	1.626	1.481	1.702	1.790
μ (mm^{-1})	0.678	5.261	0.793	5.919	6.919
R(*F*) (%)	3.26	2.16	3.47	2.62	1.65
$R_w(F^2)$ (%)	8.11	4.46	6.69	6.34	3.76

$R(F) = \sum||F_o| - |F_c||/\sum|F_o|$; $Rw(F) = [\sum w(F_o^2 - F_c^2)2/\sum w(F_o^2)^2]^{1/2}$ for $I > 2\sigma(I)$.

Table 4
Selected bond lengths (Å) and angles (°) for **3a**.

Mo–N(1)	2.197(2)
Mo–N(2)	2.322(2)
Mo′–N(2)	2.382(2)
Mo–C(1)	2.339(3)
Mo–C(2)	2.214(2)
Mo–C(3)	2.312(3)
Mo–C(4)	1.920(3)
Mo–C(5)	1.942(3)
N(1)–Mo–N(2)	36.27(7)
N(1)–Mo–N(2)′	81.51(7)
N(1)–Mo–C(4)	115.47(9)
N(1)–Mo–C(5)	85.99(9)
N(2)–Mo–N(2)′	76.54(7)
N(2)–Mo(1)–C(4)	151.71(9)
N(2)–Mo(1)–C(5)	98.43(8)
Mo–N(2)–Mo′	103.46(7)
Mo–N(1)–C(6)	131.37(16)
Mo–N(2)–C(8)	130.19(15)
Mo′–N(2)–C(8)	125.83(15)
Mo–C(4)–O(1)	174.2(2)
Mo–C(5)–O(2)	174.6(2)

Table 5
Selected bond lengths (Å) and angles (°) for **4b**.

W–N(1)	2.151(3)
W–N(2)	2.246(3)
W–N(3)	2.316(3)
W–C(9)	1.942(4)
W–C(10)	1.957(5)
W–C(11)	2.332(4)
W–C(12)	2.217(4)
W–C(13)	2.302(4)
N(1)–W–N(2)	59.61(12)
N(1)–W–N(3)	78.75(12)
N(1)–W–C(9)	99.38(15)
N(1)–W–C(10)	91.21(15)
N(2)–W–N(3)	84.34(12)
N(2)–W–C(9)	158.87(16)
N(2)–W–C(10)	97.66(15)
N(3)–W–C(9)	94.15(15)
N(3)–W–C(10)	167.09(14)
C(9)–W–C(10)	79.36(17)

Table 6
Selected bond lengths (Å) and angles (°) for **6b**.

W–N(1)	2.128(2)
W–N(2)	2.118(2)
W–C(11)	1.942(3)
W–C(12)	1.937(3)
W–C(13)	2.331(3)
W–C(14)	2.184(3)
W–C(15)	2.321(3)
N(1)–W–N(2)	62.85(8)
N(1)–W–C(11)	142.88(10)
N(1)–W–C(12)	96.28(9)
N(2)–W–C(11)	96.66(9)
N(2)–W–C(12)	139.66(9)

characterized molybdenum(II) and tungsten(II) complexes containing the *fac*-M(allyl)$(CO)_2$ fragment [1–5]. The structural features of the the *fac*-M(allyl)$(CO)_2$ moieties are very similar in **1a**, **2b**, **3a**, and **4b**. The tungsten–carbon bond lengths for the η^3-allyl ligand range between 2.202 and 2.326 Å, while the related molybdenum–carbon bond lengths lie between 2.193 and 2.343 Å. The tungsten– and molybdenum–carbon bond distances for the carbonyl ligands are between 1.940 and 1.964 Å and 1.920 and 1.955 Å, respectively. In addition to the allyl and the two carbonyl ligands, **1a**, **2b**, **3a**, and **4b** adopt various combinations of anionic

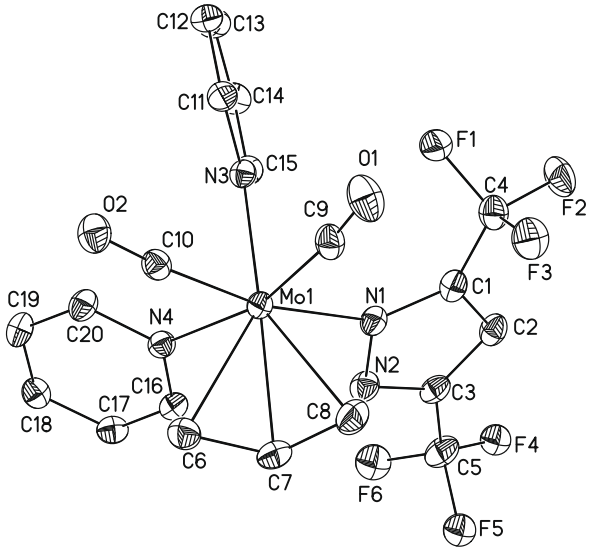

Fig. 1. Perspective view of **1a** with thermal ellipsoids at the 50% probability level.

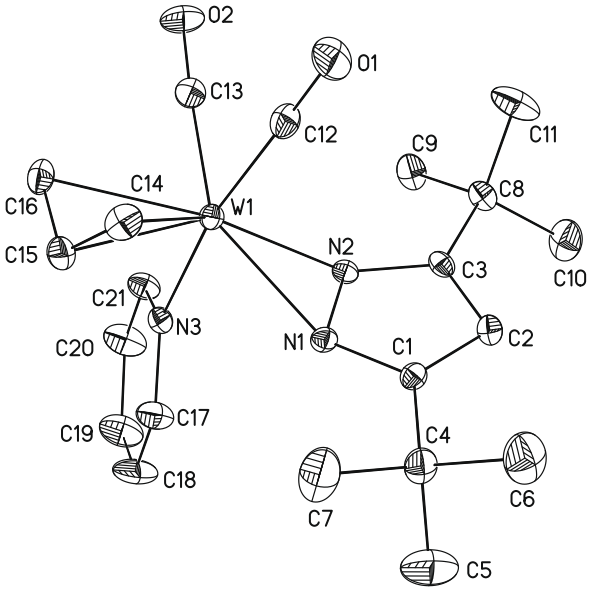

Fig. 2. Perspective view of **2b** with thermal ellipsoids at the 50% probability level.

and neutral donor ligands to satisfy the charge on the metal ions and to achieve pseudo-octahedral geometry. In **1a**, the molecular structure is obtained through coordination of two pyridine ligands and one η^1-$(CF_3)_2$pz ligand to the Mo(η^3-allyl)$(CO)_2$ fragment. The molybdenum–nitrogen bond distance for the $(CF_3)_2$pz ligand is 2.287(2) Å, while the related values for the pyridine ligands are 2.252(2) and 2.346(2) Å. The molybdenum–nitrogen bond distance for the $(CF_3)_2$pz ligand is long and comparable to those of the neutral pyridine ligands, possibly due to the electron poor nature of the pyrazolate nitrogen atom. Complex **2b** crystallizes with two independent but chemically equivalent molecules in the unit cell. Therefore, only the molecule containing W(1) is discussed herein. Pseudo-octahedral geometry in **2b** is achieved through coordination of one η^2-tBu_2pz and one pyridine ligand to the W(η^3-allyl)$(CO)_2$ fragment. η^2-Coordination of the tBu_2pz ligand leads to one less pyridine ligand, compared to **1a**. The pyrazolate tungsten–nitrogen bond distances are 2.112(2) and 2.224(2) Å. This

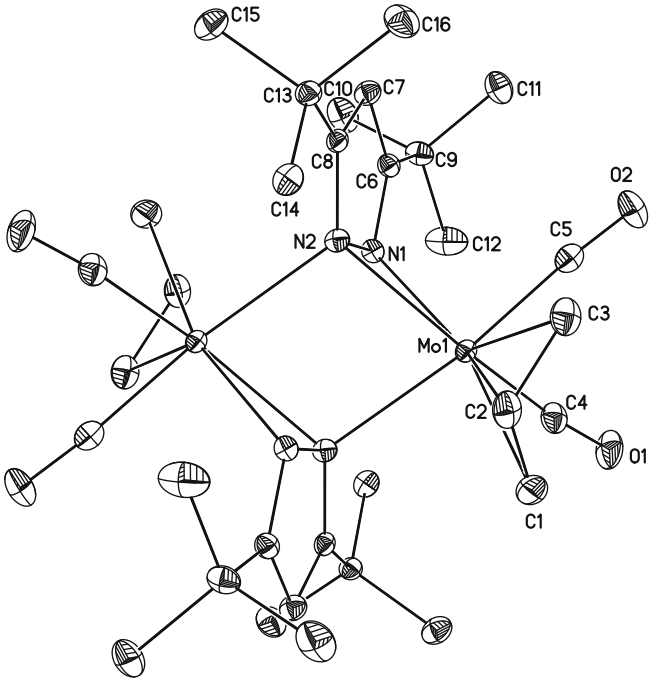

Fig. 3. Perspective view of **3a** with thermal ellipsoids at the 50% probability level.

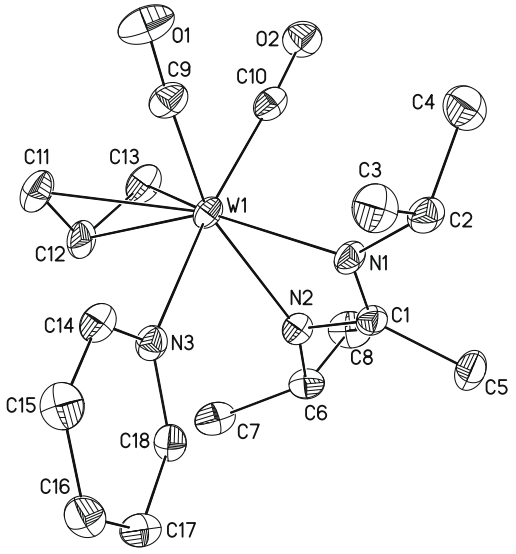

Fig. 4. Perspective view of **4b** with thermal ellipsoids at the 50% probability level.

asymmetry may be due to steric crowding between the *tert*-butyl group containing C(4) and the adjacent allyl ligand CH_2 group containing C(14). The tungsten atom lies out of the plane of the pyrazolate C_3N_2 ligand core by 1.060(3) Å, which may be driven by steric crowding between the pyridine ligand and the *tert*-butyl groups. The tungsten–nitrogen bond distance for the pyridine ligand is 2.286(2) Å, which is longer than the related values for the pyrazolate ligand, as expected for a neutral versus an anionic ligand. In **3a**, a dimeric structure results through coordination of two μ-η^1:η^2-pyrazolato ligands to the *fac*-Mo(η^3-allyl)$(CO)_2$ fragments. The dimer occupies a crystallographic inversion center. The molybdenum-nitrogen bond distances for the pyrazolate ligands are 2.197(2), 2.322(2), and 2.382(2) Å. The shortest bond distance (2.197(2) Å) is associated with the non-bridging pyrazolate nitrogen atom, while the longer two bond distances are for the pyrazo-

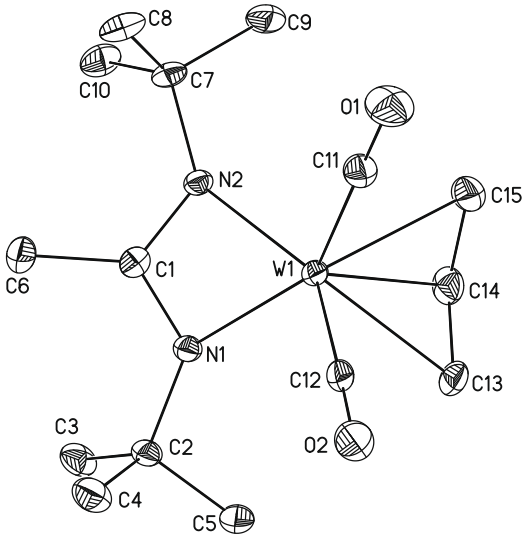

Fig. 5. Perspective view of **6b** with thermal ellipsoids at the 50% probability level.

late nitrogen atom that bridges between the two molybdenum centers. Complex **4b** achieves pseudo-octahedral geometry through coordination of one η^2-1,3-diisopropylacetamidinate and one pyridine ligand to the W(η^3-allyl)$(CO)_2$ moiety. The tungsten–nitrogen bond lengths for the amidinate ligand are 2.151(3) and 2.246(3) Å. These asymmetric bond distances may be caused by steric crowding between the isopropyl group containing C(6) and the pyridine ligand. The tungsten–nitrogen bond length for the pyridine ligand is 2.316(1) Å, which is longer than the related values for the amidinate ligand, as expected for a neutral ligand versus the anionic amidinate ligand. The N(1)–W–N(2) bite angle of the η^2-amidinate ligand is 59.61(12)°. The carbon–nitrogen bond lengths within the amidinate ligand CN_2 core are identical within experimental error and are consistent with delocalization of the negative charge over the CN_2 fragment.

Unlike the 18-electron complexes **1a**, **2b**, **3a**, and **4b**, the 16-electron complex **6b** adopts approximate square pyramidal geometry about the tungsten center, if the η^3-allyl ligand is considered to occupy one coordination site at the apex. Two cis-carbonyl ligands and one η^2-amidinate ligand form the base of the pyramid. The tungsten–carbon distances associated with the η^3-allyl ligand range between 2.184 and 2.331 Å, and are similar to those in **1a**, **2b**, **3a**, and **4b**. The tungsten–carbon distances for the carbonyl ligands are 1.937(3) and 1.942(3) Å, which are similar to the values in **1a**, **2b**, **3a**, and **4b**. The amidinate ligand coordinates to the tungsten center in a symmetrical η^2-fashion, with tungsten–nitrogen bond lengths of 2.118(2) and 2.128(2) Å. These values are slightly shorter than the shorter tungsten–nitrogen distance in **4b**, which may be due to lower steric crowding in 16-electron **6b** compared to 18-electron **4b**. The bite angle of the η^2-amidinate ligand is 62.85(8)°, which is slightly larger than the value in **4b** as a result of the slightly shorter tungsten–nitrogen bond lengths in **6b**. The carbon–nitrogen bond lengths within the amidinate ligand CN_2 core are identical within experimental error.

Most of the new complexes exhibited temperature-dependent NMR spectra. To understand the behavior, ^{1}H NMR spectra of **1a**, **1b**, **2a**, **2b**, **3a**, **4a**, **4b**, **5a**, **5b**, and **6b** were recorded in toluene-d_8 at various temperatures. Data are reported in the following paragraphs.

The ^{1}H NMR spectra of **1a** and **1b** were very similar to each other, suggesting similar behavior in solution. Accordingly, only the spectral data for **1a** are described. At 80 °C, **1a** exhibited resonances for the allyl ligand at δ 1.44 (d, anti-C*H*$_2$), 3.05 (d, syn-C*H*$_2$),

and 4.08 (tt, C*H*), multiplets for one type of pyridine ligand at δ 6.40, 6.82, and 8.50, and a singlet for the pyrazolate 4-hydrogen atom at δ 6.74. These data are not compatible with the solid state structure of **1a**, which should exhibit five resonances for the allyl group hydrogen atoms due to their differing chemical environments. At 23 °C, the allyl and pyridine hydrogen atom resonances were broad. At $\leqslant -20$ °C, however, sharp resonances were obtained. At −20 °C, the allyl ligand showed resonances at δ 1.40 (d, anti-CH_2), 1.54 (d, anti-CH_2), 2.63 (dd, syn-CH_2), 3.44 (dd, syn-CH_2), and 4.16 (tt, C*H*), while two types of pyridine ligand resonances were observed at δ 6.03, 6.29, 6.55, 6.63, 8.07, and 8.83. The pyrazolate 4-hydrogen atom appeared as a singlet at δ 6.82. There were no further changes in the ^{1}H NMR spectra upon cooling from −20 to −80 °C, except for small chemical shift differences. The low temperature spectra are consistent with the solid state structure, and suggest that a dynamic site exchange process is operant at higher temperatures.

The variable temperature ^{1}H NMR spectra of **2a** and **2b** were very similar, suggesting similar solution state structures. Accordingly, only the data for **2a** will be presented. At 23 °C, the ^{1}H NMR spectrum of **2a** exhibited resonances for the allyl ligand at δ 1.30 (d, anti-CH_2), 3.20 (d, syn-CH_2), and 3.66 (tt, C*H*), multiplets for the pyridine ligand at δ 6.27, 6.65, and 8.25, and singlets for the tBu_2pz ligand at δ 1.38 (C(CH_3)$_3$) and 6.00 (4-C*H*). These data are not compatible with the solid state structures of **2a** and **2b**, which require five allyl group resonances and two *tert*-butyl resonances. However, at or below −60 °C, the ^{1}H NMR spectra of **2a** exhibited resonances consistent with the solid state structure. At −80 °C, the allyl group resonances were observed at δ 1.16 (d, anti-CH_2), 1.49 (d, anti-CH_2), 3.02 (d, syn-CH_2), 3.42 (d, syn-CH_2), and 3.60 (tt, C*H*), and two *tert*-butyl resonances appeared at δ 1.35 and 1.54. The pyrazolate 4-hydrogen atom resonated at δ 6.11, and pyridine resonances were observed at δ 6.06, 6.42, and 8.19. The low temperature ^{1}H NMR spectral data suggest that a dynamic site exchange process is operant at temperatures higher than −60 °C.

At all temperatures that were examined (80 to −80 °C), **3a** exists as an approximate 80/20 mixture of two species with very similar chemical shifts. The ^{1}H NMR data were clearest at −60 °C in toluene-d_8. The major isomer showed allyl resonances at δ 0.45 (d, anti-CH_2), 2.32 (d, syn-CH_2), and 3.13 (tt, C*H*), the *tert*-butyl resonance at δ 1.50, and the pyrazolate 4-hydrogen atom resonance at δ 6.25. The minor isomer revealed allyl resonances at δ 1.31 (d, anti-CH_2), 2.92 (d, syn-CH_2), and 3.78 (tt, C*H*), the *tert*-butyl resonance at δ 1.53, and the pyrazolate 4-hydrogen atom resonance at δ 6.18. If the solid state structure is adopted in solution, it would require five separate allyl resonances, due to the differing pyrazolate coordination modes at each molybdenum center. If, however, there is a low energy dynamic process at −80 °C that equivalences the pyrazolate bonding modes at each molybdenum atom, then three allyl resonances would be observed. In this case, it is possible that the two observed isomers correspond to complexes containing anti- and syn-allyl groups across the molybdenum–molybdenum vector. It was not possible to assign the allyl group stereochemistries to the major and minor isomers.

The variable temperature ^{1}H NMR spectra of **4a** and **4b** were very similar, suggesting similar solution state structures. Only the data for **4b** will be presented. At 80 °C, the ^{1}H NMR spectrum of **4b** revealed allyl resonances at δ 1.39 (d, anti-CH_2) and 2.81 (m, overlapping syn-CH_2 and C*H*), diisopropylamidinate resonances at δ 1.08 (d, CH(CH_3)$_2$), 1.28 (s, C-CH_3), and 3.47 (septet, C*H*(CH$_3$)$_2$), and pyridine multiplets centered at δ 6.47, 6.91, and 8.73. These data are not consistent with the solid state structure of **4b**, and suggest that a dynamic process is present that allows rapid site exchange between the two types of isopropyl groups that are present in the solid state structure. Such a site exchange would also lead to the observed three allyl hydrogen atom resonances, instead of the expected five resonances. Between 60 and −20 °C, the resonances associated with the amidinate and allyl ligands broadened as the temperature was lowered. At $\leqslant -40$ °C, the ^{1}H NMR spectra were consistent with the solid state structure. At −80 °C, the ^{1}H NMR spectrum was clearest and revealed allyl resonances at δ 1.49 (d, anti-CH_2), 1.59 (d, anti-CH_2), 2.51 (m, syn-CH_2), 2.91 (tt, C*H*), and 3.40 (m, syn-CH_2), diisopropylamidinate resonances at δ 0.81 (d, CH(CH_3)(CH$_3$)′), 0.99 (d, CH(CH$_3$)(CH_3)′), 1.07 (d, CH(CH_3)″(CH$_3$)‴), 1.28 (s, C-CH_3), 1.68 (d, CH(CH$_3$)″(CH_3)‴), and 3.42 (m, 2 overlapping C*H*(CH$_3$)$_2$), and pyridine multiplets centered at δ 6.19, 6.61, and 8.69. The low temperature NMR data suggest that a dynamic site exchange process is operant at temperatures higher than −40 °C.

The variable temperature ^{1}H NMR spectra of **5a** and **5b** were very similar, suggesting similar solution state structures. Only the data for **5a** will be presented. At 23 °C, **5a** revealed allyl resonances at δ 1.29 (d, anti-CH_2), 3.54 (m, syn-CH_2), and 3.74 (tt, C*H*), singlets for the amidinate ligand at δ 1.10 (C(CH_3)$_3$) and 1.66 (C-CH_3), and pyridine ligand resonances centered at δ 6.54, 6.88, and 9.04. The spectra did not change upon warming to 80 °C and cooling to −80 °C, except for small changes in chemical shifts with temperature. X-ray crystal structure determinations were not carried out for **5a** or **5b**, so the solid state structures are not known. However, the ^{1}H NMR spectra of **5b** suggest a solution structure in which the two carbonyl ligands and the two nitrogen atoms of the amidinate ligand comprise the equatorial plane of an octahedron, while the allyl and pyridine ligands occupy the axial positions. Such a structure differs from the solid state structures of **4a** and **4b**, and appears to arise from better accommodation of both of the bulky amidinate *tert*-butyl groups in the equatorial plane, as opposed to spanning axial and equatorial sites, as in **4a** and **4b**.

The ^{1}H NMR spectra of **6b** also indicated a static structure between 60 and −80 °C, and only small chemical shift changes were observed with changes in temperature. For example, at −40 °C, allyl resonances were observed at δ 1.09 (d, anti-CH_2), 2.59 (tt, C*H*), and 2.66 (m, syn-CH_2), while singlets for the amidinate ligand appeared at δ 1.19 (C(CH_3)$_3$) and 1.58 (C-CH_3). These spectral data suggest a solution structure between 60 and −80 °C that is similar to the solid state structure.

The results described herein demonstrate that **1a**, **1b**, **2a**, **2b**, **4a**, and **4b** exist in non-symmetric structures in the solid state, in which there is not a plane of symmetry passing through the central carbon atoms of the allyl ligands. Previous work has demonstrated that similar non-symmetric structures predominate in molybdenum and tungsten complexes containing the *fac*-M(allyl)(CO)$_2$ fragment [1–5]. Molecular orbital calculations of *fac*-[Mo(allyl)(CO)$_2$(2,2′-bipyridine)(NCH)]$^+$ predicted that the non-symmetric isomer in which the 2,2′-bipyridine ligand nitrogen atoms span one axial and one equatorial site is 2 kJ/mol lower in energy than the symmetrical isomer where the 2,2′-bipyridine ligand nitrogen atoms both lie in the equatorial plane [4g]. As such, the non-symmetrical isomers appear to be slightly favored thermodynamically over the symmetrical isomers, which is supported herein by the crystal structures and NMR spectral data for **1a**, **1b**, **2a**, **2b**, **4a**, and **4b**. By contrast, the di-*tert*-butylacetamidate complexes **5a** and **5b** adopt symmetrical structures, even though the closely related **4a** and **4b** have non-symmetrical structures in the solid state and in solution. This difference is almost certainly related to the differences in steric bulk between the *tert*-butyl and isopropyl substituents. In **4a** and **4b**, the isopropyl groups are small enough so that they can be accommodated in one axial and one equatorial coordination site. In **5a** and **5b**, the larger *tert*-butyl groups restrict coordination of the two amidinate nitrogen atoms to two equatorial sites, where the steric constraints are presumably lower. The complexes M(allyl)(PhNCHNPh)(CO)$_2$(L) (L = py, M = Mo, W; L = PEt$_3$, M = W) adopt symmetrical solid state

structures in which the formamidinate ligand nitrogen atoms are coordinated to two equatorial sites [2a]. However, unlike the static ^{1}H NMR spectra observed for **5a** and **5b**, the ^{1}H NMR spectrum of Mo(allyl)(PhNCHNPh)$(CO)_2$(py) at −60 °C exhibited a 4:1 ratio of the symmetrical and unsymmetrical isomers.

It was proposed that the pyridine ligand is very labile in M(allyl)(PhNCHNPh)$(CO)_2$(py), and that pyridine ligand loss leads to the highly reactive 16-electron fragment M(allyl)(PhNCHNPh)$(CO)_2$ [2a]. Pyridine loss and formation of a 16-electron square pyramidal intermediate were also proposed to account for dynamic site exchange of the acetylacetonate methyl groups in Mo(allyl)$(CH_3COCHCOCH_3)(CO)_2$(py) [4h]. Other site exchange mechanisms have been proposed in related complexes containing *fac*-M(allyl)$(CO)_2$ moieties [13]. In the present work, we have isolated and structurally characterized the stable 16-electron complexes **6a** and **6b**. The complexes were obtained in low yields upon sublimation of **5a** and **5b**, and confirm the pyridine ligand lability in **5a** and **5b**. The isolation of **6a** and **6b** and observation of dynamic ^{1}H NMR spectra in **1a**, **1b**, **2a**, **2b**, **4a**, and **4b** suggest that pyridine dissociation leads to stereochemically non-rigid 16-electron species that can access structures with a plane of symmetry that passes through the central carbon atom of the allyl ligand and the 4-carbon atom of the pyrazolate ligands (**1a**, **1b**, **2a**, **2b**) or the central carbon atom of the diisopropylamidinate ligand (**4a**, **4b**). Complexes **4a** and **4b** would require two pyridine loss/square pyramidal intermediate **9** formation/pyridine recoordination cycles to allow for complete site exchange of the isopropyl methyl groups. In **1a** and **1b**, the $(CF_3)_2$pz ligand adopts an η^1-coordination mode in the solid state. Pyridine loss may lead to 18-electron intermediates **7** containing η^2-$(CF_3)_2$pz ligands (Scheme 1), with structures similar to those of **2a** and **2b**. Structure **7** contains a plane of symmetry that would lead to the observed site exchange. Pyridine loss in **2a** and **2b** could afford monomeric 16-electron species **8** that contain an η^2-tBu_2pz ligand, which has a mirror plane that passes through the 4-pyrazolate carbon atom and central carbon atom of the allyl ligand. Alternatively, pyridine loss from **2a** and **2b** could lead to dimeric **3a** and the tungsten analog, which also have a mirror plane that would afford site exchange. Pyridine loss from **4a** and **4b** probably leads to 16-electron intermediates **9** with structures that are very similar to the solid state structure of **6b**. Sublimation of **4a** and **4b** led to extensive solid state decomposition and some vapor transport of intact **4a** and **4b**. Stable 16-electron complexes with structures similar to those of **6a** and **6b** were not observed, probably because the diisopropylamidinate ligand is not bulky enough to provide kinetic stabilization of the reactive unsaturated metal centers. Finally, we note that our mechanistic studies of the exchange processes are not definitive, since more detailed efforts were beyond the scope of this investigation

The new complexes were evaluated for their volatility and thermal stability. In preparative sublimations (∼0.5 g), complexes **1a**, **1b**, **2a**, **2b**, **4a**, and **4b** sublimed at 90, 95, 125, 135, 100, 125 °C/0.03 Torr, respectively, and afforded **1a**, **1b**, **2a**, **2b**, **4a**, and **4b** in 20–45% recovered yields. The ^{1}H and ^{13}C{^{1}H} NMR spectrum of the sublimed complexes were identical to the materials before sublimation, demonstrating that no reaction occurred during the vapor transport processes. However, there were 35–60% residues at the completion of the sublimations, indicating that significant decomposition took place during sublimations. Complex **3a** was the most thermally stable among the series. Sublimation of **3a** on a 0.52 g scale at 170 °C/0.03 Torr afforded sublimed **3a** in 71% recovered yield. There was a 16% non-volatile residue at the completion of the sublimation, indicating that some thermal decomposition was concurrent with vapor transport. Consistent with competitive thermal decomposition during the sublimation process, a 6% yield of sublimed 3,5-di-*tert*-butylpyrazole (tBu_2pzH) was also isolated. The melting behavior of **3a** was carefully examined. Several crystals of **3a** were sealed in a melting point capillary tube under argon, and the sample was heated at 1 °C per minute in a melting point apparatus. The yellow crystals of **3a** began to darken between 182 and 189 °C, and melting with decomposition was observed between 190 and 193 °C. Hence, the solid state decomposition of **3a** starts at about 182 °C. The thermogravimetric analysis trace of **3a** under nitrogen at atmospheric pressure exhibited complex behavior most likely associated with concurrent thermal decomposition and volatilization. The majority of the weight loss occurred between 100 and 300 °C, with two distinct events starting at about 100 and 180 °C. The first weight loss event is probably associated with the onset of volatilization, and the second event likely corresponds to the onset of thermal decomposition. There was a 45% residue at 400 °C.

The pyridine-containing complexes **1a**, **1b**, **2a**, **2b**, **4a**, **4b**, **5a**, and **5b** sublimed partially, but also underwent extensive decomposition in the solid state during the sublimation processes. Like the dynamic site exchange processes outlined above, the solid state decompositions are probably initiated by pyridine loss to afford reactive 16-electron species. Due to the low decomposition temperatures and high non-volatile residues, **1a**, **1b**, **2a**, **2b**, **4a**, **4b**, **5a**, and **5b** are not promising film growth precursors for CVD or ALD, at least with conventional thermal precursor delivery. The most thermally stable complex reported herein is **3a**, which shows evidence for decomposition in the solid state starting at 182 °C with a heating rate of 1 °C per minute. The higher thermal stability and better vapor transport of **3a**, compared to **1a**, **1b**, **2a**, **2b**, **4a**, **4b**, **5a**, and **5b**, appears to be associated with its lack of pyridine ligands. Use of the amidinate–carbonyl complex Ru(tBuNC(Me)N$tBu)_2(CO)_2$ in the ALD growth of ruthenium metal films has been described [14]. This precursor shows an increasing growth rate with increasing temperatures above 200 °C, in both ALD and CVD growth modes. Little or no film growth was observed below 200 °C. These observations suggest that the film growth is partially or substantially assisted by thermal decomposition of Ru(tBuNC(Me)N$tBu)_2(CO)_2$, and that the onset of thermal decomposition is at about 200 °C. The most likely thermal decomposition reaction for Ru(tBuNC(Me)N$tBu)_2(CO)_2$ is carbonyl loss. The similarity of decomposition temperatures for **3a** and Ru(tBuNC(Me)N$tBu)_2(CO)_2$ suggests that **3a** also decomposes by carbonyl loss. Interestingly, pyridine-free **6b** melts with decomposition at about 180 °C, and this process may also be initiated by carbonyl loss.

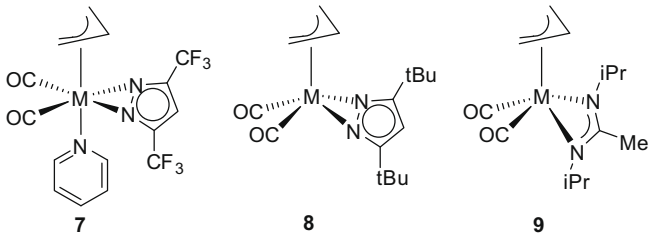

Scheme 1. Proposed monomeric intermediates involved in the dynamic site exchange processes for **1a**, **1b**, **2a**, **2b**, **4a**, and **4b**.

3. Experimental

3.1. General considerations

All reactions were carried out under argon using either glovebox or Schlenk line techniques. Toluene was distilled from sodium, tetrahydrofuran and diethyl ether were distilled from sodium benzophenone ketyl, and hexane was distilled from P_2O_5. M(allyl)(Cl)$(CO)_2(py)_2$ (M = Mo, W) [11], M(allyl)(Cl)$(CO)_2(NCCH_3)_2$ [12], and tBu_2pzK [15] were prepared by literature procedures. $(CF_3)_2$pzK

was prepared from $(CF_3)_2$pzH and KH in tetrahydrofuran, following the method described for tBu_2pzK [15]. $(CF_3)_2$pzH, methyllithium, 1,3-diisopropylcarbodiimide, and 1,3-di-*tert*-butylcarbodiimide were purchased from Aldrich Chemical Company and used as received. ^{1}H, ^{13}C{^{1}H}, and ^{19}F NMR were obtained in benzene-d_6 or toluene-d_8 on 500, 400, or 300 MHz spectrometers. Infrared spectra were obtained using Nujol as the medium. Elemental analyses were performed by Midwest Microlab, Indianapolis, IN. Melting points were obtained with a Haake-Buchler HBI digital melting point apparatus or an Electrothermal Model 9200 melting point apparatus and are uncorrected. Thermogravimetric analyses were conducted on a Perkin Elmer Pyris 1 TGA system between 25 and 500 °C, using nitrogen as the flow gas with a heating rate of 10 °C/min.

3.2. Preparation of Mo(allyl)((CF$_3$)$_2$pz)(CO)$_2$(py)$_2$ (**1a**)

A 100-mL Schlenk flask, equipped with a magnetic stir bar and a rubber septum, was charged with Mo(allyl)(Cl)$(CO)_2py_2$ (1.00 g, 2.59 mmol) and tetrahydrofuran (40 mL) and was cooled to −78 °C. To this solution was added a solution of $(CF_3)_2$pzK (0.651 g, 2.67 mmol) in tetrahydrofuran (20 mL). The resultant yellow solution was stirred at ambient temperature for 18 h. The solvent was then removed under reduced pressure to yield a yellow crystalline solid. This solid was extracted with toluene (40 mL) and the resultant solution was filtered through a 2-cm pad of Celite on a coarse glass frit. Removal of the volatile components under reduced pressure, followed by vacuum drying for 1 h, afforded **1a** as a yellow crystalline solid (0.978 g, 68%): m.p. 145–147 °C; IR (Nujol, cm^{-1}) 1944 (ν_{CO}, vs), 1847 (ν_{CO}, vs); ^{1}H NMR (toluene-d_8, 80 °C, δ) 8.50 (s, 4H, $H_{2,6}$ of py), 6.82 (m, 2H, H_4 of py), 6.74 (s, 1H, pz ring C*H*), 6.40 (m, 4H, $H_{3,5}$ of py), 4.08 (tt, J = 9.8, 6.6 Hz, 1H, allyl-C*H*), 3.04 (d, J = 6.6 Hz, 2H, allyl-CH_2), 1.43 (d, J = 9.6 Hz, 2H, allyl-CH_2); ^{13}C{^{1}H} (toluene-d_8, 80 °C, ppm) 226.82 (s, *C*O), 153.20 (s, $C_{2,6}$ of py), 142.29 (q, $^2J_{CF}$ = 39 Hz, *C*-CF_3), 137.27 (s, C_4 of py), 124.03 (s, $C_{3,5}$ of py), 121.53 (q, $^1J_{CF}$ = 270.2 Hz, *C*F_3), 104.91 (s, pz ring *C*H), 75.21 (s, allyl-*C*H), 61.08 (s, allyl-*C*H_2); ^{19}F NMR (toluene-d_8, 21 °C, ppm) 127.51 (br s, CF_3).

Anal. Calc. for $C_{20}H_{16}F_6MoN_4O_2$: C, 43.37; H, 3.02; N, 9.75. Found: C, 43.34; H, 2.91; N, 10.11%.

3.3. Preparation of W(allyl)((CF$_3$)$_2$pz)(CO)$_2$(py)$_2$ (**1b**)

In a fashion similar to the preparation of **1a**, treatment of W(allyl)$(CO)_2(py)_2$ (1.00 g, 2.10 mmol) with $(CF_3)_2$pzK (0.511 g, 2.10 mmol) in tetrahydrofuran (40 mL) afforded **1b** as a yellow crystalline solid (1.35 g, 81%): m.p. 152–153 °C; IR (Nujol, cm^{-1}) 1937 (ν_{CO}, s), 1826 (ν_{CO}, s); ^{1}H NMR (toluene-d_8, 80 °C, δ) 8.54 (br s, 4H, $H_{2,6}$ of py), 6.87 (m, 2H, H_4 of py), 6.71 (s, 1H, pz ring C*H*), 6.40 (br s, 4H, $H_{3,5}$ of py), 3.31 (tt, J = 9.8, 6.6 Hz, 1H, allyl-C*H*), 2.81 (br s, 2H, allyl-CH_2), 1.75 (d, J = 9.3 Hz, 2H, allyl-CH_2); ^{13}C{^{1}H} (toluene-d_8, 80 °C, ppm) 217.75 (s, *C*O), 153.65 (s, $C_{2,6}$ of py), 142.21 (q, $^2J_{CF}$ = 39 Hz, *C*-CF_3), 137.28 (s, C_4 of py), 124.44 (s, $C_{3,5}$ of py), 121.42 (q, $^1J_{CF}$ = 270.2 Hz, *C*F_3), 105.25 (s, pz ring *C*H), 66.50 (s, allyl-*C*H), 53.44 (s, allyl-*C*H_2); ^{19}F NMR (toluene-d_8, 21 °C, ppm) 128.57 (br s, CF_3), 125.50 (br s, CF'_3).

Anal. Calc. for $C_{20}H_{16}F_6N_4O_2W$: C, 37.41; H, 2.51; N, 8.72. Found: C, 37.53; H, 2.53; N, 8.71%.

3.4. Preparation of Mo(allyl)tBu2pz)(CO)$_2$(py) (**2a**)

In a fashion similar to the preparation of **1a**, treatment of Mo(allyl)(Cl)$(CO)_2(py)_2$ (1.00 g, 2.59 mmol) with tBu_2pzK (0.571 g, 2.61 mmol) in tetrahydrofuran (40 mL) afforded **2a** as a yellow-brown crystalline solid (0.932 g, 80%): m.p. 176–178 °C; IR (Nujol, cm^{-1}) 1941 (ν_{CO}, s), 1842 (ν_{CO}, s); ^{1}H NMR (benzene-d_6, 21 °C, δ) 8.19 (m, 2H, $H_{2,6}$ of py), 6.54 (m, 1H, H_4 of py), 6.12 (m, 2H, $H_{3,5}$ of py), 6.00 (s, 1H, pz ring C*H*), 3.62 (tt, J = 9.9, 6.6 Hz, 1H, allyl-C*H*), 3.16 (d, J = 6.6 Hz, 2H, allyl-CH_2), 1.34 (s, 18H, C(CH_3)$_3$), 1.29 (d, J = 9.9 Hz, 2H, allyl-CH_2); ^{13}C{^{1}H} (benzene-d_6, 21 °C, ppm) 231.07 (s, *C*O), 161.47 (s, *C*C(CH$_3$)$_3$), 150.94 (s, $C_{2,6}$ of py), 136.90 (s, C_4 of py), 124.06 (s, $C_{3,5}$ of py), 102.05 (s, pz ring *C*H), 73.44 (s, allyl-*C*H), 54.35 (s, allyl-*C*H_2), 32.26 (s, *C*(CH$_3$)$_3$), 30.85 (s, C(CH$_3$)$_3$).

Anal. Calc. for $C_{21}H_{29}MoN_3O_2$: C, 55.87; H, 6.48; N, 9.31. Found: C, 55.73; H, 6.55; N, 9.49%.

3.5. Preparation of W(allyl)(tBu$_2$pz)(CO)$_2$(py) (**2b**)

In a fashion similar to the preparation of **1a**, treatment of W(allyl)(Cl)$(CO)_2(py)_2$ (1.00 g, 2.10 mmol) with tBu_2pzK (0.458 g, 2.10 mmol) in tetrahydrofuran (40 mL) afforded **2b** as a red crystalline solid (0.883 g, 78%): m.p. 178–180 °C; IR (Nujol, cm^{-1}) 1931 (ν_{CO}, s), 1828 (ν_{CO}, s); ^{1}H NMR (benzene-d_6, 21 °C, δ) 8.29 (m, 2H, $H_{2,6}$ of py), 6.59 (m, 1H, H_4 of py), 6.18 (m, 2H, $H_{3,5}$ of py), 6.12 (s, 1H, pz ring C*H*), 3.02 (br s, 2H, allyl-CH_2), 2.90 (tt, J = 9.6, 6.6 Hz, 1H, allyl-C*H*), 1.60 (br s, 2H, allyl-CH_2), 1.30 (s, 18H, C(CH_3)$_3$); ^{13}C{^{1}H} (benzene-d_6, 21 °C, ppm) 221.07 (br s, *C*O), 160.79 (s, *C*C(CH$_3$)$_3$), 151.44 (s, $C_{2,6}$ of py), 137.23 (s, C_4 of py), 124.53 (s, $C_{3,5}$ of py), 103.83 (s, pz ring *C*H), 65.00 (s, allyl-*C*H), 46.93 (s, allyl-*C*H_2), 32.36 (s, *C*(CH$_3$)$_3$), 30.68 (s, C(CH$_3$)$_3$).

Anal. Calc. for $C_{21}H_{29}N_3O_2W$: C, 46.77; H, 5.42; N, 7.79. Found: C, 46.69; H, 5.32; N, 7.88%.

3.6. Preparation of [Mo(allyl)(tBu$_2$pz)(CO)$_2$]$_2$ (**3a**)

In a fashion similar to the preparation of **1a**, treatment of Mo(allyl)(Cl)$(CO)_2(NCCH_3)_2$ (2.00 g, 6.43 mmol) with tBu_2pzK (1.42 g, 6.50 mmol) in tetrahydrofuran (40 mL) afforded **3a** as a dark yellow crystalline solid (1.91 g, 79%): m.p. 190–193 °C (dec); IR (Nujol, cm^{-1}) 1935 (ν_{CO}, s), 1845 (ν_{CO}, s); ^{1}H NMR (toluene-d_8, 80 °C, δ) major isomer: 6.34 (s, 1H, pz ring C*H*), 3.63 (tt, J = 9.3, 7.2 Hz, 1H, allyl-C*H*), 3.22 (d, J = 7.2 Hz, 2H, allyl-CH_2), 1.32 (s, 18H, C(CH_3)$_3$), 1.09 (d, J = 9.3 Hz, 2H, allyl-CH_2); ^{13}C{^{1}H} (toluene-d_8, 80 °C, ppm) major isomer: 234.01 (s, *C*O), 162.99 (s, *C*C(CH$_3$)$_3$), 109.03 (s, pz ring *C*H), 78.78 (s, allyl-*C*H), 54.59 (s, allyl-*C*H_2), 32.92 (s, *C*(CH$_3$)$_3$), 30.54 (s, C(*C*H$_3$)$_3$); at 80 °C, the ^{1}H resonances of the minor isomer were partially obscured by those of the major isomer, and the carbon resonances of the minor isomer were not resolved in the ^{13}C{^{1}H} spectrum.

Anal. Calc. for $C_{32}H_{46}N_4O_4Mo_2$: C, 51.76; H, 6.24; N, 7.54. Found: C, 51.79; H, 6.34; N, 7.62%.

3.7. Preparation of Mo(allyl)(iPrNC(Me)NiPr)(CO)$_2$(py) (**4a**)

A 100-mL Schlenk flask, equipped with a magnetic stir bar and a rubber septum, was charged with 1,3-diisopropylcarbodiimide (0.41 mL, 2.65 mmol) and diethyl ether (30 mL). To this stirred solution at ambient temperature was added a 1.6 M solution of methyllithium in diethyl ether (1.66 mL, 2.66 mmol). The resultant colorless solution was stirred at ambient temperature for 2 h. This solution was added by a cannula to a separate 100-mL Schlenk flask that was cooled to −78 °C containing Mo(allyl)(Cl)$(CO)_2(py)_2$ (1.00 g, 2.59 mmol) suspended in tetrahydrofuran (40 mL). The resultant orange-red solution was warmed to room temperature and was stirred for 18 h. The volatile components were then removed under reduced pressure to yield a yellow crystalline solid. This solid was extracted with toluene (40 mL), and the resultant solution was filtered through a 2-cm pad of Celite on a coarse glass frit. The filtrate was concentrated to about 20 mL under reduced pressure and was placed in a −20 °C freezer for 36 h. Decanting of the solvent followed by vacuum drying afforded yellow crystals of **4a** (0.941 g, 87%): m.p. 125–127 °C; IR (Nujol, cm^{-1}) 1917 (ν_{CO},

s), 1818 (ν_{CO}, s); ^{1}H NMR (toluene-d_8, 80 °C, δ) 8.65 (m, 2H, $H_{2,6}$ of py), 6.93 (m, 1H, H_4 of py), 6.51 (m, 2H, $H_{3,5}$ of py), 3.77 (tt, J = 9.3, 6.3 Hz, 1H, allyl-C*H*), 3.42 (septet, J = 6.2 Hz, 2H, C*H*(CH_3)$_2$), 3.06 (d, J = 6.9 Hz, 2H, allyl-CH_2), 1.34 (s, 3H, C(CH_3)), 1.17 (d, J = 9.3 Hz, 2H, allyl-CH_2), 1.08 (d, 12H, J = 6.6 Hz, CH(CH_3)$_2$); ^{13}C{^{1}H} (toluene-d_8, 21 °C, ppm) 229.78 (s, *C*O), 168.89 (N_2CCH_3), 151.87 (s, $C_{2,6}$ of py), 136.87 (s, C_4 of py), 123.74 (s, $C_{3,5}$ of py), 68.68 (s, allyl-*C*H), 56.10 (s, allyl-CH_2), 48.15 (*C*H(CH_3)$_2$), 24.55 (CH(*C*H_3)$_2$), 10.33 (N_2CCH_3).

Anal. Calc. for $C_{18}H_{27}MoN_3O_2$: C, 52.30; H, 6.58; N, 10.17. Found: C, 52.50; H, 6.46; N, 10.23%.

3.8. Preparation of W(allyl)(iPrNC(Me)NiPr)(CO)$_2$(py) (**4b**)

In a fashion similar to the preparation of **4a**, treatment of W(allyl)(Cl)(CO)$_2$(py)$_2$ (1.00 g, 2.10 mmol) with Li(iPrNC(Me)NiPr) (prepared from a 1.6 M solution of methyllithium in diethyl ether (1.35 mL, 2.16 mmol) and 1,3-diisopropylcarbodiimide (0.32 mL, 2.10 mmol)) in tetrahydrofuran at −78 °C afforded **4b** as a yellow crystalline solid (0.933 g, 79%): m.p. 150–152 °C; IR (Nujol, cm^{-1}) 1905 (ν_{CO}, s), 1803 (ν_{CO}, s); ^{1}H NMR (toluene-d_8, 80 °C, δ) 8.74 (m, 2H, $H_{2,6}$ of py), 6.91 (m, 1H, H_4 of py), 6.48 (m, 2H, $H_{3,5}$ of py), 3.47 (septet, J = 6.9 Hz, 2H, C*H*(CH_3)$_2$), 2.84 (br, 3H, overlapping allyl-C*H*, allyl-CH_2), 1.39 (d, J = 6.0 Hz, 2H, allyl-CH_2), 1.28 (s, 3H, C(CH_3)), 1.07 (d, 12H, J = 6.0 Hz, CH(CH_3)$_2$); ^{13}C{^{1}H} (toluene-d_8, 60 °C, ppm) 222.13 (s, *C*O), 169.63 (N_2CCH_3), 152.33 (s, $C_{2,6}$ of py), 136.97 (s, C_4 of py), 124.01 (s, $C_{3,5}$ of py), 60.59 (s, allyl-*C*H), 48.32 (s, allyl-CH_2), 48.09 (s, *C*H(CH_3)$_2$), 24.33 (s, CH(*C*H_3)$_2$), 11.54 (s, N_2CCH_3).

Anal. Calc. for $C_{18}H_{27}N_3O_2W$: C, 43.13; H, 5.43; N, 8.38. Found: C, 43.52; H, 5.36; N, 8.25%.

3.9. Preparation of Mo(allyl)(tBuNC(Me)NtBu)(CO)$_2$(py) (**5a**)

In a fashion similar to the preparation of **4a**, treatment of Mo(allyl)(Cl)(CO)$_2$(py)$_2$ (1.00 g, 2.59 mmol) with Li(tBuNC(Me)NtBu) (0.456 g, 0.259 mmol) afforded **5a** (0.835 g, 73%) as yellow crystals: m.p. 120–122 °C; IR (Nujol, cm^{-1}) 1912 (ν_{CO}, s), 1811 (ν_{CO}, s); ^{1}H NMR (toluene-d_8, 21 °C, δ) 9.04 (br s, 2H, $H_{2,6}$ of py), 6.88 (m, 1H, H_4 of py), 6.54 (m, 2H, $H_{3,5}$ of py), 3.74 (br s, 1H, allyl-C*H*), 3.53 (br s, 2H, allyl-CH_2), 1.66 (s, 3H, C(CH_3)), 1.29 (d, J = 9.3 Hz, 2H, allyl-CH_2), 1.10 (s, 18H, C(CH_3)$_3$); ^{13}C{^{1}H} (toluene-d_8, 21 °C, ppm) 229.70 (s, *C*O), 171.11 (N_2CCH_3), 152.83 (s, $C_{2,6}$ of py), 137.30 (s, C_4 of py), 123.68 (s, $C_{3,5}$ of py), 72.82 (s, allyl-*C*H), 57.88 (s, *C*(CH$_3$)$_3$), 51.92 (s, allyl-CH_2), 33.03 (C(*C*H_3)$_3$), 21.76 (N_2CCH_3).

Anal. Calc. for $C_{20}H_{31}MoN_3O_2$: C, 54.42; H, 7.08; N, 9.52. Found: C, 54.21; H, 7.02; N, 9.61%.

3.10. Preparation of W(allyl)(tBuNC(Me)tBu)(CO)$_2$(py) (**5b**)

In a fashion similar to the preparation of **4a**, treatment of W(allyl)(Cl)(CO)$_2$(py)$_2$ (1.73 g, 3.63 mmol) with Li(tBuNC(Me)tBu) afforded **5b** as a yellow crystalline solid (1.71 g, 88%): m.p. 128–130 °C; IR (Nujol, cm^{-1}) 1913 (ν_{CO}, s), 1812 (ν_{CO}, s); ^{1}H NMR (toluene-d_8, 21 °C, δ) 9.14 (br s, 2H, $H_{2,6}$ of py), 6.92 (m, H_4 of py), 6.54 (m, 2H, $H_{3,5}$ of py), 3.40 (br s, 2H, allyl-CH_2), 2.86 (br s, 1H, allyl-C*H*), 1.59 (s, 3H, C(CH_3)), 1.56 (br s, 2H, allyl-CH_2), 1.08 (s, 18H, C(CH_3)); ^{13}C{^{1}H} (toluene-d_8, 40 °C, ppm) 223.77 (s, *C*O), 172.76 (N_2CCH_3), 153.21 (s, $C_{2,6}$ of py), 138.18 (s, C_4 of py), 124.16 (s, $C_{3,5}$ of py), 66.63 (s, allyl-*C*H), 51.90 (s, *C*(CH$_3$)$_3$), 50.61 (s, allyl-CH_2), 32.95 (C(*C*H_3)$_3$), 23.18 (N_2CCH_3).

Anal. Calc. for $C_{20}H_{31}N_3O_2W$: C, 45.38; H, 5.90; N, 7.94. Found: C, 45.37; H, 5.93; N, 7.98%.

3.11. Preparation of W(allyl)(tBuNC(Me)NtBu)(CO)$_2$ (**6b**)

A 2.5 cm diameter, 30 cm long glass tube was employed for the sublimation experiment. One end of the tube was sealed and the other end was equipped with a 24/40 male joint. In an argon-filled glove box, **5b** (1.73 g) was loaded into a 1.0 × 2.5 cm glass tube and this tube was placed at the sealed end of the sublimation tube. The sublimation tube was fitted with a 24/40 vacuum adapter, and then was inserted into a horizontal Buchi Kugelrohr oven such that about 15 cm of the tube was situated in the oven. A vacuum of 0.03 Torr was established, and the oven was heated to 105 °C. Complex **6b** collected on the walls of the glass tube just outside of the heated zone as dark orange crystals that were interspersed with yellow crystals of **5b**. A sample of **6b** (0.11 g, 7%) was collected by carefully scraping the orange crystals away from the yellow crystals of **5b**, however, the crystals of **6b** were contaminated with 5–10% of **5b**: m.p. 178–180 °C; IR (Nujol, cm^{-1}) 1922 (ν_{CO}, s), 1823 (ν_{CO}, s); ^{1}H NMR (toluene-d_8, −80 °C, δ) 2.67 (d, J = 6.6 Hz, 2H, allyl-CH_2), 2.55 (m, 1H, allyl-C*H*), 1.50 (s, 3H, C(CH_3)), 1.18 (s, 18H, C(CH_3)$_3$), 1.10 (d, J = 9.9 Hz, 2H, allyl-CH_2); ^{13}C{^{1}H} (toluene-d_8, 21 °C, ppm) 230.26 (s, *C*O), 160.82 (N_2CCH_3), 65.77 (s, allyl-*C*H), 55.12 (s, *C*(CH$_3$)$_3$), 44.41 (s, allyl-CH_2), 31.47 (C(*C*H_3)$_3$), 20.18 (N_2CCH_3).

Anal. Calc. for $C_{15}H_{26}N_2O_2W$: C, 40.02; H, 5.82; N, 6.22. Found: C, 32.54; H, 6.09; N, 5.04%.

3.12. X-ray crystal structure determinations

Diffraction data were measured on a Bruker *X8 APEX-II* kappa geometry diffractometer with Mo radiation and a graphite monochromator. Frames were collected at 100 K as a series of sweeps with the detector at 40 mm and 0.3° between each frame. Frames were recorded for 5–10 s. APEX-II [16] and SHELX-97 [17] software were used in the collection and refinement of the models.

Crystals of **1a** were yellow and multifaceted, and a sample of dimensions 0.20 × 0.20 × 0.16 mm^3 was used for the data collection. 61378 reflections were integrated, of which 6958 were independent. Hydrogen atoms were placed in observed positions. The fluorine atoms in one CF_3 group were disordered in two positions and were assigned partial occupancies and isotropic thermal parameters. Complex **2b** crystallized as yellow irregular fragments. A sample with dimensions of 0.20 × 0.12 × 0.10 mm^3 was used for the data collection. 84,817 reflections were harvested, of which 14,548 were unique. Hydrogen atoms were placed in calculated or observed positions. The asymmetric unit contains two independent mononuclear species. The dimeric complex **3a** crystallized as yellow flat rods. A crystal sized 0.16 × 0.06 × 0.015 mm^3 was used for the data collection. 32,345 total data points were measured, yielding 4806 independent reflections. Hydrogen atoms were observed or calculated. The asymmetric unit contains half of the neutral dimeric complex. The complex occupies a crystallographic inversion center. A yellow irregular crystal of **4b** was cut to a size of 0.16 × 0.10 × 0.08 mm^3 and yielded 20,229 measured data points, of which 4193 were independent. Hydrogen atoms were placed in observed and calculated positions. The asymmetric unit contains one neutral complex. Complex **6b** formed dark orange multifaceted crystals. The crystal mounted for data collection was 0.18 × 0.16 × 0.15 mm^3. 29,855 data points were measured, yielding 4159 independent averaged reflections. Hydrogen atoms were placed in observed and calculated positions. The asymmetric unit contains one neutral complex.

4. Supplementary material

CCDC 736967, 736968, 736969, 736970, 736971, 736972 and 736973 contain the supplementary crystallographic data for this

paper. These data can be obtained free of charge from The Cambridge Crystallographic Data Centre via www.ccdc.cam.ac.uk/data_request/cif.

Acknowledgements

We are grateful to the US National Science Foundation (Grant Nos. CHE-0314615 and CHE-0910475) for support of this research. The American University of Sharjah is acknowledged for a Faculty Research Grant (FRG08-02-28187) that paid for the travel of O.M.E.-K.

References

[1] J. Barker, M. Kilner, Coord. Chem. Rev. 133 (1994) 219–300.
[2] (a) Y. Yamaguchi, K. Ogata, K. Kobayashi, T. Ito, Inorg. Chim. Acta 357 (2004) 2657–2668;
(b) Y. Yamaguchi, K. Ogata, K. Kobayashi, T. Ito, Dalton Trans. (2004) 3982–3990;
(c) Y. Yamaguchi, K. Ogata, K. Kobayashi, T. Ito, Bull. Chem. Soc. Jpn. 77 (2004) 303–309;
(d) K. Ogata, Y. Yamaguchi, T. Kashiwabara, T. Ito, J. Organomet. Chem. 690 (2005) 5701–5709.
[3] (a) J. Pérez, D. Morales, S. Nieto, L. Riera, V. Riera, D. Miguel, Dalton Trans. (2005) 884–888;
(b) J. Pérez, E. Hevia, L. Riera, V. Riera, S. García-Granda, E. García-Rodríguez, D. Miguel, Eur. J. Inorg. Chem. (2003) 1113–1120;
(c) D. Morales, M.E.N. Clemente, J. Pérez, L. Riera, V. Riera, D. Miguel, Organometallics 22 (2003) 4124–4128;
(d) D. Morales, J. Pérez, L. Riera, V. Riera, D. Miguel, M.E.G. Mosquera, S. García-Granda, Chem. Eur. J. 9 (2003) 4132–4143;
(e) J. Pérez, L. Riera, V. Riera, S. García-Granda, E. García-Rodríguez, D. Miguel, Organometallics 21 (2002) 1622–1626.
[4] (a) F.-C. Liu, P.-S. Yang, C.-Y. Chen, G.-H. Lee, S.-M. Peng, J. Organomet. Chem. 693 (2008) 537–545;
(b) A.G.W. Hodson, S.J. Coles, M.B. Hursthouse, Polyhedron 26 (2007) 1285–1291;
(c) Y. Yamaguchi, A. Fujita, N. Suzuki, T. Ito, J. Mol. Cat. A: Chem. 240 (2005) 226–232;
(d) A.G.W. Hodson, R.K. Thind, O. Granville-George, J. Organomet. Chem. 689 (2004) 2114–2122;
(e) P.M.F.J. Costa, M. Mora, M.J. Calhorda, V. Félix, P. Ferreira, M.G.B. Drew, H. Wadepohl, J. Organomet. Chem. 687 (2003) 57–68;
(f) K.-H. Yih, G.-H. Lee, Y. Wang, Inorg. Chem. 42 (2003) 1092–1100;
(g) J.R. Ascenso, C.G. de Azevedo, M.J. Calhorda, M.A.A.F.deC.T. Carrondo, P. Costa, A.R. Dias, M.G.B. Drew, V. Félix, A.M. Galvão, C.C. Romão, J. Organomet. Chem. 632 (2001) 197–208;
(h) B.J. Brisdon, A.A. Woolf, J. Chem. Soc., Dalton Trans. (1978) 291–295.
[5] (a) J.C. Alonso, P. Neves, M.J.P. da Silva, S. Quintal, P.D. Vaz, C. Silva, A. Valente, P. Ferreira, M.J. Calthorda, V. Félix, M.G.B. Drew, Organometallics 26 (2007) 5548–5556;
(b) A.V. Malkov, L. Gouriou, G.C. Lloyd-Jones, I. Starý, V. Langer, P. Spoor, V. Vinader, P. Kočovský, Chem. Eur. J. 12 (2006) 6910–6929;
(c) J.A.R. Luft, Z.-X. Yu, D.L. Hughes, G.C. Lloyd-Jones, S.W. Krska, K.N. Houk, Tetrahedron: Asymmetry 17 (2006) 716–724;
(d) O. Belda, C. Moberg, Acc. Chem. Res. 37 (2004) 159–167;
(e) B.M. Trost, M.L. Crawley, Chem. Rev. 103 (2003) 2921–2943;
(f) S.W. Krska, D.L. Hughes, R.A. Reamer, D.J. Mathre, Y. Sun, B.M. Trost, J. Am. Chem. Soc. 124 (2002) 12656–12657;
(g) B.M. Trost, I. Hachiya, J. Am. Chem. Soc. 120 (1998) 1104–1105;
(h) B.M. Trost, M. Lautens, J. Am. Chem. Soc. 104 (1982) 5543–5545.
[6] C.L. Dezelah IV, O.M. El-Kadri, I. Szilagyi, J.L. Campbell, K. Arstila, L. Niinistö, C.H. Winter, J. Am. Chem. Soc. 128 (2006) 9638–9639.
[7] (a) R.U. Kirss, L. Meda, Appl. Organomet. Chem. 12 (1998) 155–160;
(b) S. Suh, D.M. Hoffman, L.M. Atagi, D.C. Smith, J.-R. Liu, W.-K. Chu, Chem. Mater. 9 (1997) 730–735;
(c) J.-S.M. Lehn, P. van der Heide, Y. Wang, S. Suh, D.M. Hoffman, J. Mater. Chem. 14 (2004) 3239–3245.
[8] (a) M. Ritala, M. Leskelä, in: H.S. Nalwa (Ed.), Handbook of Thin Film Materials, Academic Press, San Diego, CA, 2002, pp. 103–159;
(b) M. Leskelä, M. Ritala, Angew. Chem., Int. Ed. 42 (2003) 5548–5554;
(c) L. Niinistö, J. Päiväsaari, J. Niinistö, M. Putkonen, M. Nieminen, Phys. Status Solidi A 201 (2004) 1443–1452;
(d) M. Putkonen, L. Niinistö, Top. Organomet. Chem. 9 (2005) 125–145.
[9] (a) C.L. Dezelah IV, M.K. Wiedmann, K. Mizohata, R.J. Baird, L. Niinistö, C.H. Winter, J. Am. Chem. Soc. 129 (2007) 12370–12371;
(b) O.M. El-Kadri, M.J. Heeg, C.H. Winter, Dalton Trans. (2006) 1943–1953;
(c) O.M. El-Kadri, M.J. Heeg, C.H. Winter, Dalton Trans. (2006) 4506–4513;
[d] C.L. Dezelah IV, O.M. El-Kadri, M.J. Heeg, L. Niinistö, C.H. Winter, Proc. Electrochem. Soc. 2005-9 (2005) 563–574.
[10] (a) B.S. Lim, A. Rahtu, R.G. Gordon, Nat. Mater. 2 (2003) 749–754;
(b) B.S. Lim, A. Rahtu, J.-S. Park, R.G. Gordon, Inorg. Chem. 42 (2003) 7951–7958;
(c) J. Wu, J. Li, C. Zhou, X. Lei, T. Gaffney, J.A.T. Norman, Z. Li, R.G. Gordon, H. Cheng, Organometallics 26 (2007) 2803–2805;
(d) B. Lee, K.J. Choi, M.J. Kim, R.M. Wallace, J. Kim, Y. Senzaki, D. Shenai, H. Li, M. Rousseau, J. Suydam, Microelectron. Eng. 86 (2009) 272–276;
(e) J. Päiväsaari, C.L. Dezelah IV, D. Back, H.M. El-Kaderi, M.J. Heeg, M. Putkonen, L. Niinistö, C.H. Winter, J. Mater. Chem. 15 (2005) 4224–4233;
(f) J. Päiväsaari, J. Niinistö, P. Myllymäki, C.L. Dezelah IV, C.H. Winter, M. Putkonen, M. Nieminen, L. Niinistö, Top. Appl. Phys. 106 (2007) 15–32;
(g) B.S. Lim, A. Rahtu, P. de Rouffignac, R.G. Gordon, Appl. Phys. Lett. 84 (2004) 3957–3959;
(h) P. de Rouffignac, J.-S. Park, R.G. Gordon, Chem. Mater. 17 (2005) 4808–4814;
(i) P. de Rouffignac, A.P. Yousef, K.H. Kim, R.G. Gordon, Electrochem. Solid-St. Lett. 9 (2006) F45–F48.
[11] D.J. Bevan, R.J. Mawby, J. Chem. Soc., Dalton Trans. (1980) 1904–1909.
[12] R.G. Hayter, J. Organomet. Chem. 13 (1968) P1–P3.
[13] (a) P. Espinet, R. Hernando, G. Iturbe, F. Villafañe, A.G. Orpen, I. Pascual, Eur. J. Inorg. Chem. (2000) 1031–1038;
(b) Y.D. Ward, L.A. Villanueva, G.D. Allred, S.C. Payne, M.A. Semones, L.S. Liebeskind, Organometallics 14 (1995) 4132–4156;
(c) B.J. Brisdon, M. Cartwright, A.G.W. Hodson, M.F. Mahon, K.C. Molloy, J. Organomet. Chem. 435 (1992) 319–335;
(d) J.W. Faller, D.A. Haitko, R.D. Adams, D.F. Chodosh, J. Am. Chem. Soc. 101 (1979) 865–876;
(e) J.W. Faller, N. Sarantopoulos, Cryst. Growth Des. 5 (2005) 2356–2361.
[14] H. Li, D.B. Farmer, R.G. Gordon, Y. Lin, J. Vlassak, J. Electrochem. Soc. 154 (2007) D642–D647.
[15] C. Yélamos, M.J. Heeg, C.H. Winter, Inorg. Chem. 37 (1998) 3892–3894.
[16] APEX II Collection and Processing Programs are distributed by the Manufacturer, Bruker AXS Inc., Madison, WI, USA, 2009.
[17] G.M. Sheldrick, Acta Crystallogr. A 64 (2008) 112–122.